IEEE Access
Multidisciplinary | Rapid Review | Open Access Journal

Received 11 July 2024, accepted 26 July 2024, date of publication 6 August 2024, date of current version 2 September 2024.

Digital Object Identifier 10.1109/ACCESS.2024.3439620

RESEARCH ARTICLE

Fault Diagnosis for Inverter-Fed Motor Drives Using One Dimensional Complex-Valued Convolutional Neural Network

BOWEN CUI, SIYUAN ZHANG, JIAYI SU, AND HUAMIN CUI
School of Marine Engineering, Jimei University, Xiamen 361021, China

Corresponding author: Bowen Cui (tsuibowen@163.com)

This work was supported in part by the National Natural Science Foundation of China under Grant 51779102, and in part by Fujian Provincial Natural Science Foundation of China under Grant 2022J01811.

ABSTRACT This paper proposed a new one dimensional complex-valued convolution neural network (1D CVCNN) model to diagnose power switch open-circuit fault of three-phase inverter-fed PMSM system. The 1D CV convolution operation was defined and the CV rectified linear unit (ReLU) activation function was chosen. A CV backpropagation algorithm is also proposed for 1D CVCNN training. The 1D CVCNN framework model is built, where 1D inputs and all the weights between the layers are complex numbers. The Clarke transformation is used to process the three-phase current of the inverter to obtain a complex-valued signal. The non-overlapping sliding window sampling method is used to obtain CV data set. The fault classification accuracy of the 1D CVCNN has been verified by experiments, and the experimental results show that the 1D CVCNN has better feature extraction ability than any other conventional deep learning method and better robustness to noise.

INDEX TERMS One dimensional complex-valued convolutional neural network (1D CVCNN), fault diagnosis, open-circuit fault, three-phase inverter.

I. INTRODUCTION

Inverter-fed motor drives are widely used in various industrial applications, such as electric vehicle, aerospace, and marine electric propulsion, because of their excellent speed control and energy savings performance. The principal function of the inverter is conversion of electric energy and supply of power to the motor. The health of the inverter has a considerable impact on the safety of motor drives. Research shows that power converters account for approximately 82.5% of motor drive failures, and power switches are the most fragile components in power converters [1]. It is also estimated that about 38% of motor drives in industry are due to power switch failures [2]. Once faults occur in the inverter, the drive system will lose its ability to work normally, sometimes even resulting in a fatal accident. To improve the reliability of motor drives in safety critical applications, fault-tolerant control of the inverter is an essential requirement [3]. However, the fault-tolerant control strategy can only be implemented after isolating the faulty switch. Therefore, inverter fault diagnosis is valuable and meaningful.

In general, inverter power switch faults can be classified as short-circuit (SC) faults and open-circuit (OC) faults. As a destructive fault, SC fault can cause an abnormal overcurrent and can cause damage to other components. To avoid damage to the inverter, fast fuses are used to shut the inverter when SC fault occurred in the inverter [4], [5]. Therefore, the short-circuit fault will be an open-circuit fault, and OC faults are considered in the paper only.

Many research papers related to the diagnosis of OC fault have been published. All these OC fault diagnosis techniques can be broadly classified into three categories: model-based, signal-based, data-driven. Model-based techniques must establish a mathematical model of the drive system, and the observer is used to detect open circuit faults occurring in the inverter [6], [7], [8]. A sliding mode

The associate editor coordinating the review of this manuscript and approving it for publication was Pinjia Zhang.

observer is used to detect faulty switches in modular multilevel converters, faulty switches are isolated by comparing the observed and measured states [6]. A nonlinear observer is used to obtain residuals, a directional residual is synthesized, and the faulty switches are isolated [7]. A mixed logic dynamic model of the motor drive system is used to estimate motor currents, the current residual vector is obtained by comparing the estimator and plant, and the fault can be detected [8]. The switched linear model is set up to estimate the state of the system, the error residual between the estimates and the measured output of the converter is used to detect and identify arbitrary faults in components and sensors [9].

Signal-based techniques can be classified as voltage-based and current-based, according to the signal processed. In [10], phase currents are processed using Park's transformation and normalization, and multiple open switch faults occurring in back-to-back converters of the double-fed wind power system are diagnosed. In [11], the harmonic components of the three-phase currents are calculated, and the average values and root mean square (RMS) values of the harmonic components are used to isolate the faulty switch.

In [12], the phase voltage is calculated using the measured pole voltage, the separate residuals for each switch are defined, and the sectoral average residual is calculated for the respective switch. The faulty switch is isolated by the two residuals. In [13], voltage sensors are used to measure two line voltages, the fault phase is determined by the magnitude ratio of two line voltages, and the fault switch is located by the voltage difference. Current-based methods do not depend on system parameters and do not need additional hardware. However, these approaches need a longer time to get better diagnostic results. Voltage-based methods have a fast fault diagnostic speed, but require voltage sensors, which may substantially increase the complexity and cost of the system.

Data-driven-based techniques do not require modeling or signal processing, so they have been concerned by many researchers, and many different approaches have been delivered. In [14], the wavelet transform is used to extract the fault features, a multiple kernel extreme learning machine is applied to diagnose the fault of analog circuit. In [15], a Bayesian network-based data-driven fault diagnosis method is proposed for three-phase inverters. Fast Fourier transform (FFT) and principal component analysis (PCA) are used to generate fault features, the Bayesian network (BN) is employed to isolate the faults. In [16], a PCA-based fault diagnosis approach and the multiclass relevance vector machine (mRVM) are used for cascaded H-bridge multilevel inverter system. The methodology utilizes PCA to extract features and use the mRVM model to classify the faulty switch. In [17], an artificial neural network (ANN)-based fault diagnosis method is proposed for AC-DC converters. FFT is used to obtain fault features, and ANN is employed to isolate a fault switch. In [18], a FFT-based fault diagnosis method, relative PCA (RPCA) and support vector machine (SVM) is proposed for H-bridge multilevel inverter. Fault features are extracted using FFT and RPCA, and SVM is used to classify the faults. In [19], three-phase currents are used and fault features are generated by learning manifold features. An extreme learning machine (ELM) model is used to diagnose single and double IGBT open-circuit faults that occurred in the three-phase inverter. All these conventional data-driven methods need professional knowledge and an advanced signal processing method to extract fault features.

As a typical and predominant deep learning method, CNN was originally designed for image recognition. CNN can automatically extract features from original images without manual selection. Many researchers adopted the original two-dimensional (2D) CNN (2D CNN) for fault diagnosis. In [20], 2D images of current are used to diagnose fault of broken rotors bars in induction motors. Six CNN architectures were employed, and the study provides a comparative analysis of these CNN architectures that show high accuracies and highlights that it is not always possible to choose the best architecture based on accuracy alone. In [21], [22], and [23], the raw time-domain signals are converted into 2-D images, which are then fed into the 2D CNN model to classify the bearing fault that occurred. In [24], the one-dimensional (1D) time series current signal of the inverter is reconstructed into 2D feature maps, 2D feature maps were input into the 2D CNN for fault diagnosis. In [25], the measured current signal was processed by FFT, a hybrid CNN composed of 1D and 2D CNN is applied for fault diagnosis with a three-phase inverter, but the method needs to extract the fault features manually.

Existing traditional data-driven fault diagnosis methods need professional knowledge and advanced signal processing techniques to obtain fault characteristics. The 2D CNN-based fault diagnosis method has achieved great achievement. However, in many applications, 1D data should be converted into a 2D image to perform fault diagnosis. Most signals in practical industrial applications are 1D. If 1D signals are directly converted to 2D forms, the spatial correlation in the original sequence will be destroyed, and the information related to faults may be missing, resulting in worse performance for fault diagnosis performance.

Aimed at the problem, some researchers have employed 1D CNN to diagnose fault of inverter, motor and other equipment or device. In [26], phase current was collected and 1D CNN is used to perform motor fault diagnosis. Only one phase current was used in the study, fault features included in other two phase current were neglected. In [27], the vibration signals of the gear box were measured, 1D CNN was employed to diagnose eight fault of gear box. In the study, only the amplitude of vibration signals was considered, the phase of the signals was disregarded. In [28], phase-a current was collected by simulation, an improved 1D CNN was applied to diagnose OC fault of IGBT in the three-phase inverter. However, the samples used for network training and testing were from the simulation, and only single IGBT OC fault was considered. In [29], three-phase current of the

inverter was collected with five periods, 1D CNN was used to diagnose fault of IGBT in the three-level NPC inverter. However, the 1D data samples constructed from three-phase current results in a large amount of data, which can cost more time to train the network.

Due to considering both the phase and amplitude of the data, complex-valued CNN (CVCNN) has better performance than real-valued CNN. Reference [30] used CVCNN to solve the sleep stage classification. Reference [31] applied CVCNN for medical image denoising. However, 2D images were used in these CVCNN, and few studies have applied CVCNN to solve the problem of fault diagnosis.

Aiming at the defects and deficiencies of existing techniques, the paper constructs a 1D CVCNN model, the proposed model using 1D complex-valued data as input. Defining the 1D complex-valued convolution operation, a complex filter weight matrix, and a complex ReLU activation function, the complex backpropagation algorithm is formed. The proposed method requires neither the mathematical model of the inverter drive system nor professional signal processing methods to obtain fault features, and it can deal with complex-valued data that traditional real-valued 1D CNN cannot handle. The technique can not only realize the fault diagnosis of a system with complex-valued signal, but also deal with the fault diagnosis of a system with real-valued signal. In contrast to the traditional 1D CNN based fault diagnosis methods, the recognition accuracy has been greatly improved by 1D CVCNN. Furthermore, compared to real-valued 1D CNN, the proposed method has a higher fault diagnosis accuracy in the case of noise interference. The contributions of the paper are summarized as follows.

1) The 1D complex-valued convolution operation is defined, and the 1D complex-valued backpropagation algorithm is proposed. A novel 1D complex-valued CNN model based fault diagnosis of inverter-fed motor drives is proposed. To the best of our knowledge, there is no similar work in the literature.
2) To obtain complex-valued data for training and testing of the 1D CVCNN model, we use Clarke transformation to process the three-phase current of the inverter. The non-overlapping sliding window sampling method is used to obtain our dataset.
3) Adding white Gaussian noise with different SNR in the dataset, the model proposed in the paper works well in noise environment, and it has high accuracy of fault diagnosis under white Gaussian noise with low SNR condition.

The remainder of the paper is organized as follows. Section II briefly introduces the topology of three-phase inverter systems and defines fault labeling of IGBT open-circuit faults. Section III describes the preparation of fault data. Section IV gives the theory and architecture of 1DCVCNN. The experimental results and analysis are then shown in Section V. Finally, a general conclusion is given in Section VI.

II. INVERTER-FED PMSM DRIVES AND FAULT LABELING

The three-phase PWM inverter fed PMSM drive system is shown in Figure1. The PWM inverter is composed of six power switches (IGBT or MOSFET) V_i ($i = 1, 2, \cdots, 6$) with antiparallel diodes Di ($i = 1, 2, \cdots, 6$). Power switches whether or not conduct depend on its gate signals. The power switch conducts when the gate signal is equal to 1, otherwise, the power switch does not conduct. The power switch OC fault that occurred in the inverter means that the power switch cannot conduct whether the gate signal is equal to 1 or 0.

In practice, there may be a single or double power switch OC fault in the inverter. Therefore, the paper only considers single or double power switch OC fault. When all six switches work normally, the inverter is in a fault-free state, which is defined as a special fault mode for convenience. When a single-power switch OC fault occurred in the inverter, there are six fault modes. When a double power switch OC fault occurring in the inverter simultaneously, there are 15 fault modes. As a result, there are a total of 22 fault modes considered in the paper.

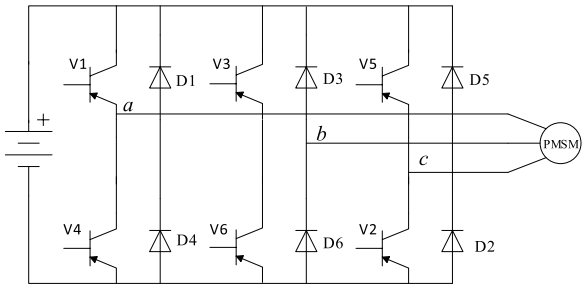

FIGURE 1. Schematic diagram of three-phase PWM inverter-fed PMSM.

Labeling each fault mode according to the location of the double power switch OC fault occurring in the inverter, the label of power switch OC fault can be listed in Table 1. Consequently, the fault diagnosis can be considered as a multiclassification problem.

TABLE 1. Labeling of inverter oc faults.

Fault modes	Label	Fault modes	Label
No fault	0	V1&V5 OC fault	11
V1 OC fault	1	V3&V5 OC fault	12
V2 OC fault	2	V4&V6 OC fault	13
V3 OC fault	3	V4&V2OC fault	14
V4 OC fault	4	V6&V2 OC fault	15
V5 OC fault	5	V1&V6 OC fault	16
V6 OC fault	6	V1&V2 OC fault	17
V1&V4 OC fault	7	V3&V4 OC fault	18
V3&V6 OC fault	8	V3&V2 OC fault	19
V5&V2 OC fault	9	V5&V4 OC fault	20
V1&V3 OC fault	10	V5&V6 OC fault	21

III. INVERTER FAULT DATA PREPARATION

When the inverter operates under fault-free condition, the three-phase currents of the inverter are symmetric

sinusoidal waves. When power switch OC faults occurred in the inverter, they became asymmetric. The phase currents of the motor are shown in Figure 2 under different power switch OC faults that occurred in the inverter. As shown in Figure 2, the waveforms of the three-phase current are different when different power switch OC faults occurred in the inverter. Therefore, the phase currents contain sufficient faulty information under different power switch OC fault conditions.

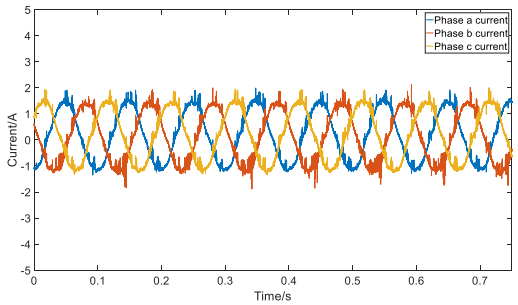

(a)

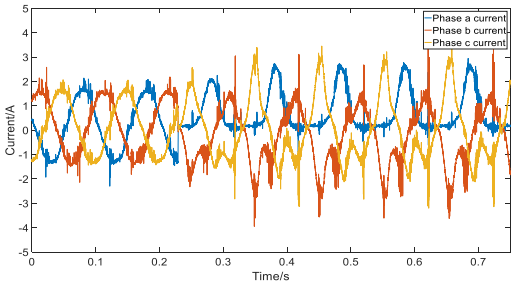

(b)

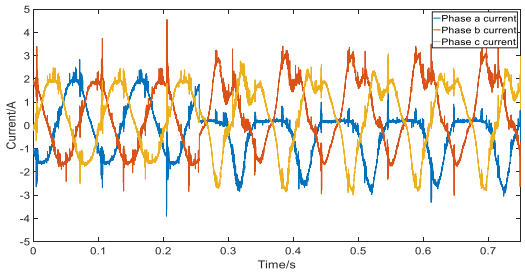

(c)

FIGURE 2. Motor phase currents under different power switch OC fault conditions of the power switch. (a) Fault-free condition. (b) Power switch V4 OC fault. (c) OC fault of the power switch V1 and V6.

When the inverter-fed PMSM drive runs normally, three-phase currents of the motor are sinusoidal waves, and the three-phase currents can be expressed as

$$\begin{cases} i_A(t) = I_m \sin(\omega t) \\ i_B(t) = I_m \sin(\omega t - 2\pi/3) \\ i_C(t) = I_m \sin(\omega t + 2\pi/3) \end{cases} \tag{1}$$

According to the research [32], the current-vector trajectories composed of the current i_α and i_β in stationary frame depends on the location of OC fault of power switch. This shows that the current i_α and i_β contain rich fault information. So the current i_α and i_β are chosen as the signal of fault.

By using the Clarke transformation, the currents i_α and i_β in stationary frame can be obtained as

$$\begin{cases} i_\alpha = \dfrac{2}{3}\left(i_A - \dfrac{1}{2}i_B - \dfrac{1}{2}i_C\right) \\ i_\beta = \dfrac{2}{3}\left(\dfrac{\sqrt{3}}{2}i_B - \dfrac{\sqrt{3}}{2}i_C\right) \end{cases} \tag{2}$$

Define the complex-valued parameter i, that is,

$$i = i_\alpha + j i_\beta \tag{3}$$

where $j = \sqrt{-1}$ is the imaginary unit. The complex-valued parameter i is used as input of the 1D CVCNN to train the network to diagnose the power switch OC fault that occurred in the inverter.

IV. THEORY OF A 1D COMPLEX-VALUED CONVOLUTIONAL NEURAL NETWORK

A. FUNDAMENTALS OF 1D CONVOLUTIONAL NEURAL NETWORK

CNN is a feedforward 2D neural network inspired by the receptive field of mammalian visual cortex cells and widely used in image and vision recognition. However, 1D CNN is a specific type of CNN where the 1D signal, 1D convolution, and subsampling are used to map features [26], [32]. Similar to 2D CNN, 1D CNN usually is composed of input layer, convolution layers, pooling layers, fully connection layers and an output layer.

The convolution layer is mainly used to extract various features of the input data by using convolution filters or kernels. The convolution layer contains a number of convolution filters or kernels, these convolution kernels can be regarded as a weight matrix. The filters slide along the time series input in a fixed stride, and the sliding filters can be considered as a moving window. At each sliding position, the weights of the filters perform a dot product with the windowed inputs and then summation. The output of the convolution can be defined as [33], [34],

$$x_k^l = b_k^l + \sum_{i=1}^{N_{l-1}} w_{ik}^{l-1} * s_i^{l-1} \tag{4}$$

where N_{l-1} is the number of kernels at layer l-1, x_k^l is the input at layer l, b_k^l is the bias of kth neural at layer l, s_i^{l-1} is the output of the ith neuron at layer l-1, w_{ik}^{l-1} is the filter from the ith neuron in layer l-1 to the kth neuron at layer l. Passing the input x_k^l through the activation function, $f(.)$, the output of the convolutional layer l can be expressed as [33],

$$y_k^L = f(x_k^l) \tag{5}$$

The pooling layer is also known as the down-sampling layer. The main function of the pooling layer is to further

extract the key feature by condensing the signal from the convolutional layer. The mainly pooling operations include max pooling and average pooling. Max-pooling is the most common method used in the pooling layer. After the down-sampling operation, the dimension of feature vectors and network parameters are reduced, and training time and memory requirements are reduced [35].

The fully connected layer is similar to a traditional multilayer neural network, which can be considered a ''classifier'' layer in the entire convolutional neural network [36], [37], [38]. The classifier is completed using the softmax function. The output of the fully connected layer is fed to the softmax function, its output logic value is mapped to a probability distribution for each class label, and the classification is performed. The softmax function can be expressed as follows:

$$\text{softmax}\,(z_i) = \frac{e^{z_i}}{\sum_{i=1}^{n} e^{z_i}} \tag{6}$$

where z_i $(i = 1, 2, \cdots, \text{n})$ denotes the output of the fully connected layer, n is the number of class labels.

B. ONE-DIMENSIONAL COMPLEX-VALUED CONVOLUTIONAL NEURAL NETWORK

The proposed 1D complex-valued convolutional neural network is termed 1D CVCNN, the structure of 1D CVCNN is shown in Figure 3. The structure includes CV convolutional layer, CV pooling layer and CV fully connected layer.

1) CONVOLUTIONAL LAYER WITH COMPLEX 1D VALUE

In the 1D CV convolution layer, a CV convolution operation is performed between the 1D CV inputs x and the CV kernel W. Suppose $x = a + jb$, $W = A + jB$, where a, b, A, B are all vectors of real value. The CV convolution operation can be expressed as follows.

$$W^* x = \left(A^* a - B^* b\right) + \left(B^* a + A^* b\right) \tag{7}$$

The schematic diagram of 1D CV convolution in CV convolution layers is shown in Figure 5. In the diagram, the CV kernel is $W \in C^{1\times 3}$, input data is $x \in C^{1\times 7}$, the stride is 1. When the CV data enter into CV convolution layers, the CV kernel move along the data in a fixed stride, which can be considered as a window (also known as local receptive field). The CV data in the window perform a dot product with the CV convolutional kernel. All the outputs computed on each window will be made up of a matrix, which is essentially a map of the input. The result of the convolution operation can be shown in Figure 4.

Forward propagation from the previous 1D CV convolution layer l–1 to the kth neuron in layer l, can be expressed as follows:

$$x_k^l = b_k^l + \sum_{i=1}^{N_{l-1}} \text{CVconv1D}\left(w_{ik}^{l-1}, s_i^{l-1}\right) \tag{8}$$

where x_k^l is the input, b_k^l is the bias of the kth neuron in layer l, s_i^{l-1} is the output of the ith neuron at layer l–1. w_{ik}^{l-1} is the 1D CV kernel from the ith neuron at layer l–1 to the kth neuron in layer l. CVconv1D $(\cdot)$ denotes 1D CV convolution operation. Passing the input x_k^l through the activation function, $\sigma(\cdot)$, the output of the kth neuron at the convolutional layer l can be expressed as follows,

$$y_k^l = \sigma\left(\text{Re}\left(x_k^l\right)\right) + j\sigma\left(\text{Im}\left(x_k^l\right)\right) \tag{9}$$

2) COMPLEX-VALUED ACTIVATION FUNCTION

In a convolution neural network, to enhance the ability to express nonlinearity, the activation function is applied to

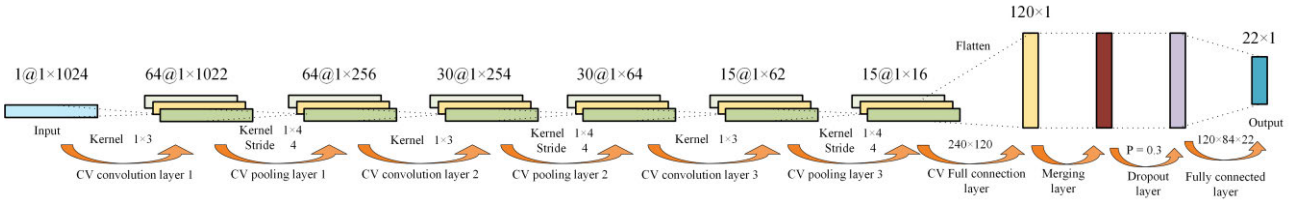

FIGURE 3. The schematic diagram of 1D CV convolution.

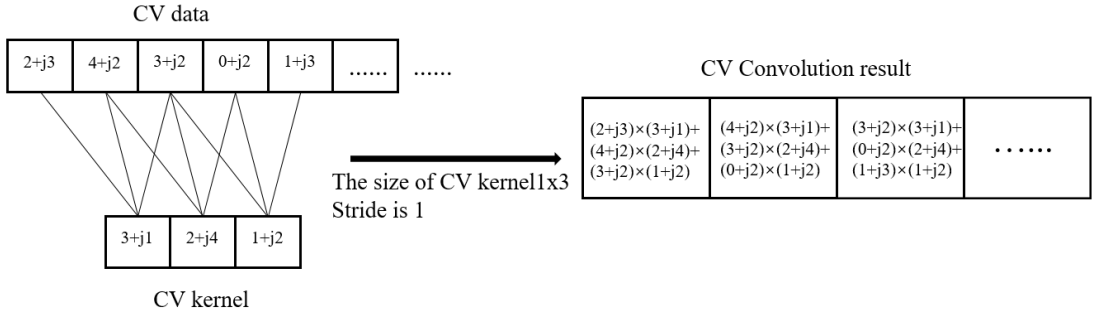

FIGURE 4. The schematic diagram of 1D CV convolution.

the output of the convolution layer to perform a non-linear transformation. The Rectified Linear Unit (ReLU) function is a widely used activation function for real-valued CNN. To solve the nonlinearity existed in complex-valued data, complex-valued activation function should be considered in the 1D CVCNN. Considering the superior performance of the ReLU in real-valued CNN, the CReLU activation function is applied in the paper by extending the real-valued ReLU in the complex-valued field. CReLU simply applies the standard ReLU activation function to the real and imaginary part of the input z, which can be defined as follows [39].

$$\mathrm{CReLU} = \mathrm{ReLU}\left(\mathrm{Re}\left(z\right)\right) + j\,\mathrm{ReLU}\left(\mathrm{Im}\left(z\right)\right) \tag{10}$$

where Re(·) and Im(·) denote the real and imaginary parts, respectively.

3) COMPLEX-VALUED POOLING LAYER

In the real-valued pooling layer, the corresponding feature of the data is extracted by comparing the data values. However, there is no rule for directly comparing complex numbers, so it is necessary to define the rule for the complex-valued pooling algorithm.

A complex number is composed of the real imaginary part; the real and imaginary part of the data can be analyzed and processed respectively when training the network, so the maximum complex number can be determined after comparing the size of the real imaginary part of the complex number, respectively. Maximum pooling and average pooling for complex numbers are defined as follows.

$$X_{CPL} = \mathrm{MaxPooling}\left(\mathrm{Re}\left(Z_{CC}\right)\right) + j\,\mathrm{MaxPooling}\left(\mathrm{Im}\left(Z_{CC}\right)\right) \tag{11}$$

$$X_{CAL} = \mathrm{AvgPooling}\left(\mathrm{Re}\left(Z_{CC}\right)\right) + j\,\mathrm{AvgPooling}\left(\mathrm{Im}\left(Z_{CC}\right)\right) \tag{12}$$

where Z_{CC} is the output of the convolution layer, X_{CPL}, X_{CAL} are output of the maximum pooling and average pooling layer, respectively.

4) FULLY CONNECTED COMPLEX-VALUED LAYER

Similarly to real-valued (RV) CNN, CV CNN contains one or more fully connected layers. The fully connected layers are the same as a traditional multilayer perception, which are usually applied to extract features further. The output of the CV fully connected layer can be described as:

$$\begin{aligned} O_i^{l-1} &= \sigma\left(\mathrm{Re}\left(V_i^{l-1}\right)\right) + j\sigma\left(\mathrm{Im}\left(V_i^{l-1}\right)\right) \\ &= \mathrm{Re}\left(V_i^{l-1}\right) + j\,\mathrm{Im}\left(V_i^{l-1}\right) \end{aligned} \tag{13}$$

$$V_i^{l-1} = \sum_{k=1}^{K} W_{ik}^{l} \cdot X_k^{l-1} + b_k^{l} \tag{14}$$

where σ is the activation function, W_{ik}^{l} is the kernel from the ith neuron in layer lth to the kth neuron at layer $l+1$. b_k^{l} denotes the bias of the kth neuron at layer l, X_k^{l-1} denotes the kth output of the (l-1)th layer, K is the number of neurons at layer l-1.

5) MERGING LAYER

After the complex-valued fully connected layer, the merging layer is followed. The main function of merging layer is to calculate the magnitude of the kth element of the complex feature vector in the CV fully-connected layer. The output of the merging layer can be expressed as follows [31],

$$O_i^{L} = abs\left(O_i^{L-1}\right) = \sqrt{\left(\mathrm{Re}\left(O_i^{L-1}\right)\right)^2 + \left(\mathrm{Im}\left(O_i^{L-1}\right)\right)^2} \tag{15}$$

where O_i^{L-1} is the i th element of the complex feature vector in CV fully connected layer.

6) DROPOUT LAYER

When training the networks, if the model has too many parameters and too few training samples, the trained model is prone to overfitting. The Dropout layer can effectively alleviate the problem of overfitting during training and achieve regularization to a certain extent. Some layers are discarded randomly after Dropout operation by setting probability coefficients of the Dropout layer.

Because the dropout layer randomly discards some neurons probability, it weakens the forced joint relationship between neural nodes between layers, thereby enhancing the network's generalization ability and making the relationships between neurons in the network more independent. The dropout layer also reduces the mutual adaptability between neurons and improves the effectiveness of the features extracted by CNN.

7) OUTPUT LAYER

After the RV fully-connected layer, the output layer is usually followed to predict the classification of the input data. The LogSoftmax function is used in classification due to its better numerical performance compared to SoftMax [40]. The LogSoftMax function can convert the feature vector into a normalized probability distribution. Mathematically, the output of Logsoftmax classification for the ith element of the vector can be calculated by the LogSoftmax operation and can be described as

$$q_i = \log\left(\frac{\exp\left(O_i^{L}\right)}{\sum_{k=1}^{N}\exp\left(O_k^{L}\right)}\right) \tag{16}$$

where q_i is the probability belonging to the ith class for one complex training sample, N is the number of classes.

C. BACK PROPAGATION FOR 1D CVCNN

Backpropagation in CNN with complex number is an extension of the 1D real-valued counterpart in which the loss function and activations are required to be differentiable

by the real and imaginary parts of the complex-valued parameters [31]. The objective of the BP in 1D CVCNN is to optimize the network parameters by minimizing the value of the loss function.

For multiclass classification, the loss function is applied to evaluate the difference between the predicted value and the actual value of the model. The cross-entropy loss function is the most widely used loss function in multiclass classification, which is good at learning information and converges quickly, which can be defined as follows [41],

$$L_{CE} = -\sum_{i=1}^{N} p_i \log q_i \tag{17}$$

where N is the number of classes, p_i denotes the probability distribution of the training data, q_i denotes the probability distribution generated by the network.

The 1D CVCNN is trained by minimizing the value of the loss function L_{CE}, and this can be done using Adam optimizer [42]. The minimum of the loss function is reached by adjusting the complex weights and bias iteratively as follows.

$$w_{ik}^{l+1}(t+1) = w_{ik}^{l+1}(t) - \eta \frac{\partial L_{CE}}{\partial w_{ik}^{l+1}(t)} \tag{18}$$

$$b_{ik}^{l+1}(t+1) = b_{ik}^{l+1}(t) - \eta \frac{\partial L_{CE}}{\partial b_{ik}^{l+1}(t)} \tag{19}$$

where η is the learning rate, t is the number of iterations. The update of weights and bias are similar. Here, only the update of weights is considered. The complex error gradient of weights can be obtained as

$$\begin{aligned}\frac{\partial L_{CE}}{\partial w_{ik}^{l+1}} &= \frac{\partial L_{CE}}{\partial \mathrm{Re}\left(w_{ik}^{l+1}\right)} + j\frac{\partial L_{CE}}{\partial \mathrm{Im}\left(w_{ik}^{l+1}\right)} \\ &= \left(\frac{\partial L_{CE}}{\partial \mathrm{Re}\left(V_i^{l+1}\right)}\frac{\partial \mathrm{Re}\left(V_i^{l+1}\right)}{\partial \mathrm{Re}\left(w_{ik}^{l+1}\right)} + \frac{\partial L_{CE}}{\partial \mathrm{Im}\left(V_i^{l+1}\right)}\frac{\partial \mathrm{Im}\left(V_i^{l+1}\right)}{\partial \mathrm{Re}\left(w_{ik}^{l+1}\right)}\right) \\ &\quad + j\left(\frac{\partial L_{CE}}{\partial \mathrm{Re}\left(V_i^{l+1}\right)}\frac{\partial Re\left(V_i^{l+1}\right)}{\partial \mathrm{Im}\left(w_{ik}^{l+1}\right)} + \frac{\partial L_{CE}}{\partial \mathrm{Im}\left(V_i^{l+1}\right)}\frac{\partial \mathrm{Im}\left(V_i^{l+1}\right)}{\partial \mathrm{Im}\left(w_{ik}^{l+1}\right)}\right)\end{aligned} \tag{20}$$

According to [36] and [37], (20) can be changed to

$$\begin{aligned}\frac{\partial L_{CE}}{\partial w_{ik}^{l+1}} &= \left(\frac{\partial L_{CE}}{\partial \mathrm{Re}\left(V_i^{l+1}\right)} + j\frac{\partial L_{CE}}{\partial \mathrm{Im}\left(V_i^{l+1}\right)}\right) \\ &\quad \times \left(\mathrm{Re}\left(O_k^l\right) - j\,\mathrm{Im}\left(O_k^l\right)\right) \\ &= -\delta_i^{l+1}\bar{O}_i^l\end{aligned} \tag{21}$$

where

$$\delta_i^{l+1} = \frac{\partial L_{CE}}{\partial \mathrm{Re}\left(V_i^{l+1}\right)} + j\frac{\partial L_{CE}}{\partial \mathrm{Im}\left(V_i^{l+1}\right)}$$

is called the error term, $\bar{O}_k^l = \mathrm{Re}\left(O_k^l\right) - j\,\mathrm{Im}\left(O_k^l\right)$, which is the conjugate of the ith output of the lth layer.

According to (18), (19), and (21), in the process of back-propagation, the complex weight and bias of each layer can be obtained by multiplying the error term with the conjugate of the input of this layer. The detail of error term of different layer of the CV CNN will be given below.

1) OUTPUT LAYER

The backward error term of the output layer can be calculated by differentiating both sides of (17) with respect to O_i^L

$$\begin{aligned}\delta_k^L &= \frac{\partial L_{CE}}{\partial O_i^L} = \sum_{j=1}^{N}\frac{\partial L_{CE}}{\partial q_j}\frac{\partial q_j}{\partial O_i^L} = -\sum_{j=1}^{N}\frac{p_j}{q_j}\left(\delta_{ij}q_j - q_i q_j\right) \\ &= -\sum_{j=1}^{N} p_j\left(\delta_{ij} - q_i\right) = q_i - p_i\end{aligned} \tag{22}$$

where δ_{ij} is 1 if i is equal to j and 0 otherwise.

2) MERGING LAYER

The backward error term of the merging layer can be calculated by differentiating the loss function from the layer output O_i^{L-1}, the error term can be expressed as follows [41],

$$\begin{aligned}\delta_k^{L-1} &= \frac{\partial L_{CE}}{\partial O_k^{L-1}} = \frac{\partial L_{CE}}{\partial \mathrm{Re}(O_k^{L-1})} + j\frac{\partial L_{CE}}{\partial \mathrm{Im}(O_k^{L-1})} \\ &= \frac{\partial L_{CE}}{\partial O_k^L}\frac{\partial O_k^L}{\partial \mathrm{Re}e(O_k^{L-1})} + j\frac{\partial L_{CE}}{\partial O_k^L}\frac{\partial O_k^L}{\partial \mathrm{Im}(O_k^{L-1})} \\ &= \delta_k^L\frac{\mathrm{Re}(O_k^{L-1})}{O_k^L} + \delta_k^L\frac{\mathrm{Im}(O_k^{L-1})}{O_k^L} \\ &= \delta_k^L\cos\varphi + j\delta_k^L\sin\varphi\end{aligned} \tag{23}$$

where $\varphi = \arctan(\mathrm{Im}(O_k^{L-1})/\mathrm{Re}(O_k^{L-1}))$, δ_k^{L-1} is the complex error term.

3) FULLY CONNECTED COMPLEX-VALUED LAYER

For updating the bias and all weights in the layer, one can use the chain rule of derivatives by differentiating the loss function LCE with respect to the CV connection weights and bias. Suppose that the L-2 layer is output layer of CV fully connected layer, then the previous layer L-3 is called hidden layer, and the error δ_k^{L-2} can be expanded as

$$\begin{aligned}&\delta_i^{l+1} \\ &= \frac{\partial L_{CE}}{\partial V_{ik}^{L-1}} = \frac{\partial L_{CE}}{\partial \mathrm{Re}\left(V_{ik}^{L-1}\right)} + j\frac{\partial L_{CE}}{\partial \mathrm{Im}\left(V_{ik}^{L-1}\right)} \\ &= \left(\frac{\partial L_{CE}}{\partial \mathrm{Re}(O_i^{L-1})}\frac{\partial \mathrm{Re}(O_i^{L-1})}{\partial \mathrm{Re}\left(V_{ik}^{L-1}\right)} + \frac{\partial L_{CE}}{\partial \mathrm{Im}(O_i^{L-1})}\frac{\partial \mathrm{Im}(O_i^{L-1})}{\partial \mathrm{Re}\left(V_{ik}^{L-1}\right)}\right)\end{aligned}$$

$$+j\left(\frac{\partial L_{CE}}{\partial \mathrm{Re}(O_i^{L-1})}\frac{\partial \mathrm{Re}(O_i^{L-1})}{\partial \mathrm{Im}\left(V_{ik}^{L-1}\right)}+\frac{\partial L_{CE}}{\partial \mathrm{Im}(O_i^{L-1})}\frac{\partial \mathrm{Im}(O_i^{L-1})}{\partial \mathrm{Im}\left(V_{ik}^{L-1}\right)}\right)$$
$$=\delta_k^L\left(\cos\varphi\frac{\partial \mathrm{Re}(O_i^{L-1})}{\partial \mathrm{Re}\left(V_{ik}^{L-1}\right)}+\sin\varphi\frac{\partial \mathrm{Im}(O_i^{L-1})}{\partial \mathrm{Re}\left(V_{ik}^{L-1}\right)}\right)$$
$$+j\delta_k^L\left(\cos\varphi\frac{\partial \mathrm{Re}(O_i^{L-1})}{\partial \mathrm{Im}\left(V_{ik}^{L-1}\right)}+\sin\varphi\frac{\partial \mathrm{Im}(O_i^{L-1})}{\partial \mathrm{Im}\left(V_{ik}^{L-1}\right)}\right) \tag{24}$$

where,

$$\frac{\partial \mathrm{Re}\left(O_i^{l-1}\right)}{\partial \mathrm{Re}\left(V_{ik}^{l-1}\right)}=\frac{\partial \mathrm{Im}\left(O_i^{l-1}\right)}{\partial \mathrm{Im}\left(V_{ik}^{l-1}\right)}=1,$$
$$\frac{\partial \mathrm{Re}\left(O_i^{l-1}\right)}{\partial \mathrm{Im}\left(V_{ik}^{l-1}\right)}=\frac{\partial \mathrm{Im}\left(O_i^{l-1}\right)}{\partial \mathrm{Re}\left(V_{ik}^{l-1}\right)}=0.$$

(24) can be expressed as,

$$\delta_i^{l+1}=\delta_k^{L-1}=\delta_k^L\cos\varphi+j\delta_k^L\sin\varphi \tag{25}$$

The error term δ_i^l can be deduced as,

$$\delta_k^L=-\frac{\partial L_{CE}}{\partial \mathrm{Re}\left(O_k^L\right)}-j\frac{\partial L_{CE}}{\partial \mathrm{Im}\left(O_k^L\right)}.$$

On the basis of the chain rule,

$$\delta_k^l=\frac{\partial L_{CE}}{\partial O_k^l}=-\delta_i^{l+1}\overline{w_{ik}^{l+1}}$$
$$=\sum_{i=1}^{I}\left[\mathrm{Re}\left(\delta_i^{l+1}\right)\mathrm{Re}\left(w_{ik}^{l+1}\right)+\mathrm{Im}\left(\delta_i^{l+1}\right)\mathrm{Im}\left(w_{ik}^{l+1}\right)\right]$$
$$-j\sum_{i=1}^{I}\left[\mathrm{Im}\left(\delta_i^{l+1}\right)\mathrm{Re}\left(w_{ik}^{l+1}\right)+\mathrm{Re}\left(\delta_i^{l+1}\right)\mathrm{Im}\left(w_{ik}^{l+1}\right)\right] \tag{26}$$

where $\overline{(\cdot)}$ represents operation of the complex conjugate.

From the process of the deriving the error term of hidden layers, we can see that the error terms can be derived from the parameters of upper layers [42], [43], [44]. Similarly, the error terms of the convolution layer and the pooling layer can be obtained.

4) ERROR TERM OF THE CONVOLUTIONAL LAYER AND POOLING LAYER

Similarly, the error term expressions of the convolution layer and the pooling layer can be obtained. The method for solving the error item of the convolution layer is the same as the method for solving the error term of the hidden layer, we get the following.

$$\delta_k^l=\beta_i^{l+1}\left[\mathrm{Re}\left(\delta_i^{l+1}\right)+\mathrm{Im}\left(\delta_i^{l+1}\right)\right]$$
$$+j\beta_i^{l+1}\left[\mathrm{Im}\left(\delta_i^{l+1}\right)-\mathrm{Re}\left(\delta_i^{l+1}\right)\right] \tag{27}$$

where β is the pooling factor. Similarly, get the error term of the pooling layer:

$$\delta_k^l=\sum_{i=1}^{I}\left[\mathrm{Re}\left(\delta_i^{l+1}\right)\mathrm{Re}\left(w_{ik}^{l+1}\right)+\mathrm{Im}\left(\delta_i^{l+1}\right)\mathrm{Im}\left(w_{ik}^{l+1}\right)\right]$$
$$+j\sum_{i=1}^{I}\left[\mathrm{Im}\left(\delta_i^{l+1}\right)\mathrm{Re}\left(w_{ik}^{l+1}\right)+\mathrm{Re}\left(\delta_i^{l+1}\right)\mathrm{Im}\left(w_{ik}^{l+1}\right)\right] \tag{28}$$

After obtaining the error terms for each layer, the weights and bias of each layer are updated.

$$w_{ik}^{l+1}(t+1)=w_{ik}^{l+1}(t)+\eta\delta_i^{l+1}\overline{O_i^l} \tag{29}$$
$$b_{ik}^{l+1}(t+1)=b_{ik}^{l+1}(t)+\eta\delta_i^{l+1} \tag{30}$$

The weights and bias are adjusted iteratively until the loss function is reduced to the minimum while the network training is completed. The flowchart of the model training is shown in Figure 5.

V. EXPERIMENT RESULTS

A. DESCRIPTION OF THE EXPERIMENT

The connection diagram of the experimental rig is shown in Figure 6, the permanent magnet synchronous motor (PMSM) is coaxially connected with the separately excited DC machine (SEDM), and the SEDM is used as the load of the PMSM. The power inverter is composed of six IGBT (G60N100BNTD of Fairchild). The computer is used to run the PLECS software together with the RT Box. The RT Box is used as a digital controller to send the pulse-width modulation (PWM) logic signals to the gate drive circuits that drive the inverter switches. The experimental parameters are shown in Table 2.

The number of layers and main structural parameters of the 1D CVCNN proposed in the paper are shown in Table 3. It should be noted that the hyperparameters of the network are set as follows: the number of iterations is set to 50, the optimizer is Adam algorithm, the learning rate is 0.001, $\beta_1 = 0.9, \beta_2 = 0.999$. The Dropout is set 0.3. All experiments are performed in computer with CPU i7-10700 @ 2.9GHz with eight cores and 16 GB of memory, and NVIDIA GeForce RTX 2060(6G) GPU, running on a Windows 10 professional 64-bit operating system. Python is chosen as the programming language, Pycharm2020.2 is used for programming.

B. DATA PREPARING

In this paper, the non-overlapping sliding window sampling method is used to intercept the original three-phase current signal data to make a sample set, and the moving step is equal to the sliding window size. As shown in Figure 7,

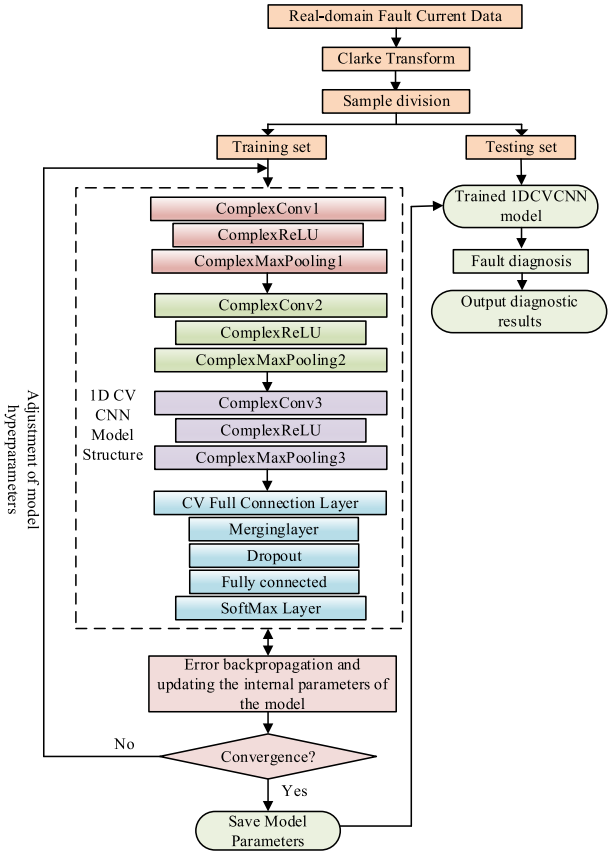

FIGURE 5. Flowchart of the model training.

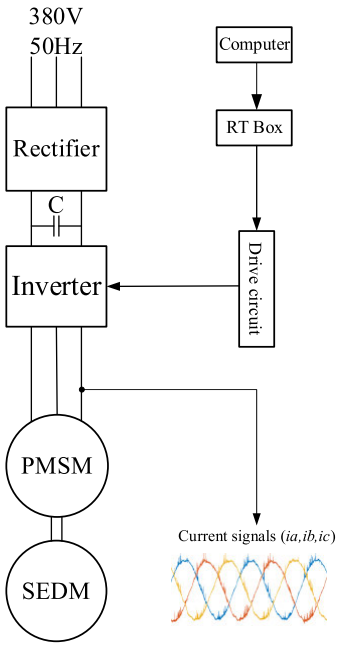

FIGURE 6. Connection diagram of the experimental rig.

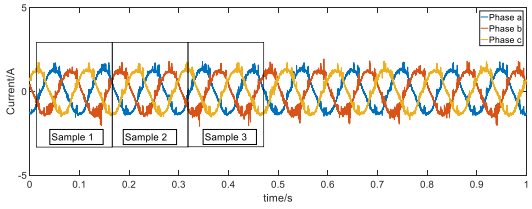

FIGURE 7. Data preparation with non-overlapping sampling.

take the i_a current waveform with inverter under fault-free condition as an example, each sample has 1024 sampling points, and the sliding window size is 1024. The sample is cut from left to right through the non-overlapping sliding window, and 1.1×10^5 sampling points of current are divided into 1000 samples. For each type of fault, 800 samples are taken as the training set and 200 samples are taken as the testing set. The dataset description of each fault is shown in Table 3.

The same sampling method is used to process the current i_α and i_β. After finishing i_α, i_β current sampling, the train and test sample sets can be obtained by using expression (3).

C. DETECTION PERFORMANCE EVALUATION

To verify the effectiveness of the 1D CVCNN model, real motor current data samples are used to train the model. Figure 9 illustrates the convergence history of the accuracy and loss function for the training during 50 epochs. When the number of training is 10, the accuracy and loss function of the model reaches 95% and 0.2, respectively. The loss function value tends to zero and the accuracy tends to 1 with increasing training iteration. The loss value and the accuracy of the model converge and are stable even after 50 epochs.

To analyze the fault identification performance of the proposed method, the confusion matrix of the 1D CVCNN is shown in Figure 9. In the figure, the vertical axis indicates the actual fault label, and the horizontal axis denotes the predicted fault label. The diagonal number of the matrix represents the diagnostic precision of each fault. The lowest diagnostic accuracy of fault 12, 17 reaches 99%, and the other fault can be isolated with an accuracy of 100%. The experimental results show that the proposed method has a good performance in fault diagnosis and has the ability to accurately classify the faulty power switch. The reason for

TABLE 2. Experimental parameters of PMSM drives.

parameter	Value
Rated voltage of PMSM	200V
Rated current of PMSM	6.2A
Rated power of PMSM	1.5kWr
Rated speed of PMSM	1500rpm
Number of pole pairs of PMSM	2
Stator phase resistance of PMSM	1.2Ω
d-axis inductance	3.72mH
q-axis inductance	7.28mH
Permanent magnetic flux linkage	0.4534Wb
Load	2Nm
Switching frequency of IGBT	18kHz
Sampling frequency	20kHz

TABLE 3. Dataset description of each fault.

Fault label	Dataset train/test	Fault label	Dataset train/test
0	800/200	11	800/200
1	800/200	12	800/200
2	800/200	13	800/200
3	800/200	14	800/200
4	800/200	15	800/200
5	800/200	16	800/200
6	800/200	17	800/200
7	800/200	18	800/200
8	800/200	19	800/200
9	800/200	20	800/200
10	800/200	21	800/200

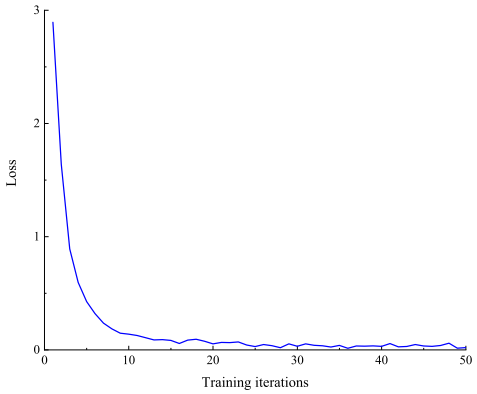

(a)

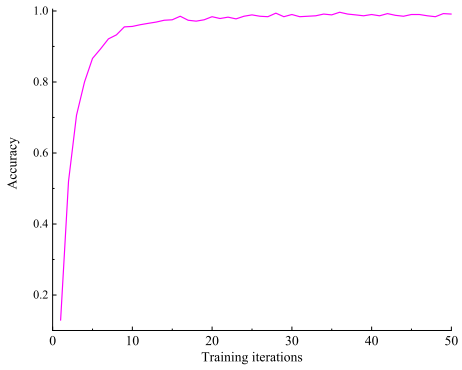

(b)

FIGURE 8. The convergence history. (a) accuracy. (b) loss.

the good performance of the 1D CVCNN model is that complex-valued current consider both amplitude and phase simultaneously.

D. COMPARED TO 1D CNN MODELS UNDER SIGNAL WITH DIFFERENT NOISE

To evaluate the superiority of the anti-noise ability, noises with different SNR (SNR = 5, 10, 20dB) are added to the dataset. The diagnostic accuracy of the 1D CVCNN and the 1D CNN are shown in Figure 10. From the figure, we can see that the diagnostic accuracy of the 1D CVCNN is 93.4%, the 1D CNN is 91.6%, when the SNR drops to 5dB.

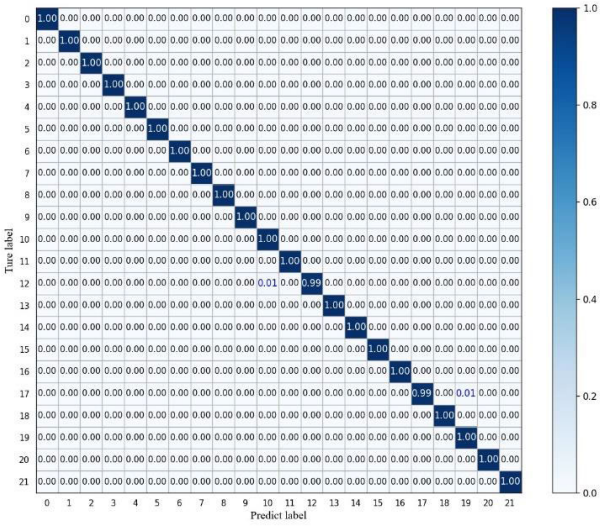

FIGURE 9. Fault diagnosis confusion matrix without noise.

The comparison shows that the 1D CVCNN method proposed in this work performs better than the 1D CNN in the noise interference environment.

To evaluate more comprehensive performance of the 1D CVCNN model compared with the other models, the receiver operating characteristic (ROC) curve at SNR = 5dB is shown in Figure 11. In the figure, the horizontal ordinate denotes the false positive rate (FPR), the vertical ordinate denotes the true positive rate (TPR), and the area under ROC curve (AUC) are utilized to evaluate the comprehensive detection performance. The larger the value of AUC means the better the performances of the model [41]. From the figure, we can see that the AUC of the 1D CVCNN is 0.99, the 1D CNN is 0.98, the BP is 0.89, and the DNN is 0.84. The AUC of the 1D CVCNN is the largest, which means that the method proposed in the paper is the most effective under noisy environments.

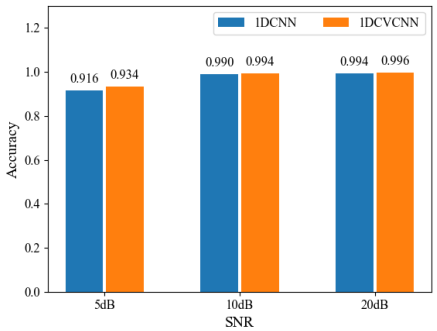

FIGURE 10. Average accuracy of 1D CVCNN and 1D CNN with different SNR noise.

E. TRAINING EFFICIENCY COMPARISON WITH OTHER METHODS

To further illustrate the training efficiency of the proposed method, the diagnosis accuracy of the proposed method (1D CVCNN) is compared with existing conventional methods,

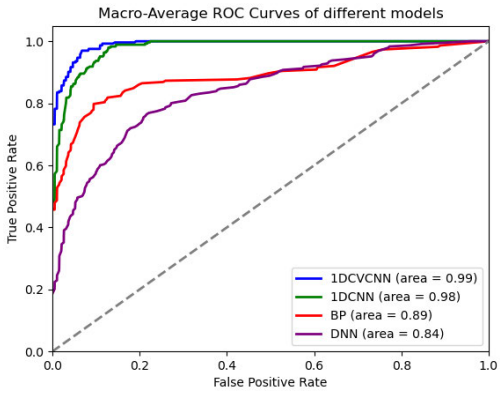

FIGURE 11. ROC curves of different models under signal with SNR = 5dB noise.

such as 1DCNN, real-valued deep network (DNN), real-valued BP network (BP) in 50 training epochs. The comparison results are shown in Figure 12. From the Figure 14, it can be seen that the diagnosis accuracy of all four methods improves as the number of epochs increases.

The diagnostic precision of the 1D CVCNN is 98.4%, and the 1D CNN is 97.4%, the DNN is 88.6% and BP is only 74% after ten epochs. The diagnosis accuracy of the 1D CVCNN is 99.4% and 1D CNN is 98.9%, DNN is 98.6% and BP is only 82% after 20 epochs. After 40 epochs, the accuracy of 1D CVCNN,1D CNN and DNN exceeds 99%. However, from the comparison results, we can see that the accuracy of 1D-CVCNN has reached 99.4% after only 10 epochs. Therefore, 1D CVCNN has better feature extraction ability and higher efficiency compared to 1D CNN, BP networks, and DNNs.

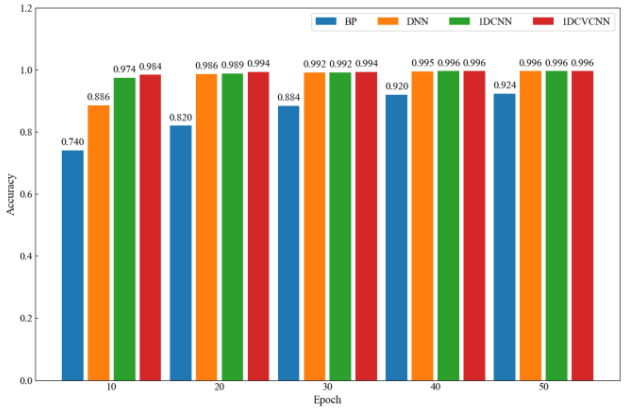

FIGURE 12. Accuracy of 1D CVCNN and other conventional models.

For further comparison, the training time of the above algorithm is shown in Table 4. It shows that the proposed method has a longer training time than other algorithms. The main reason for the long training time of complex convolution is that it requires more time than real convolution. However, the proposed method has more accuracy than other algorithms under noise interference conditions. Due to unavoidable environmental noise interference, therefore, we think that the proposed method still has the best result.

TABLE 4. Comparing of train time of different algorithm.

Algorithm	Configuration	Training time (s)
BP	1 hidden layer with 1200 nodes	52.95
DNN	3 hidden layers with 1200,500,120 noses, respectively	65.92
1DCNN	3 convolution, pooling and full connected layers, 1 dropout layer,1 softmax layer	46.44
1DCVCNN	The same as above	84.64

VI. CONCLUSION

This paper proposed a new 1D complex-valued CNN model to diagnose the power switch OC fault of the three-phase inverter-fed PMSM system. The model can automatically extract the feature from the original phase current. The experiments were carried out on 1D CVNN, 1D CNN, BP and DNN models with 22 kinds of power switch OC faults occurs in the inverter. The main contributions of the study are shown as follows:

1) The complex-valued phase current can directly be used as the input of the trained 1D CVCNN model. The power switch OC fault diagnosis can be implemented with the model.
2) The 1D CVCNN has a higher diagnosis accuracy than 1D CNN and has better feature extraction ability than other conventional deep learning methods, such as BP and DNN.
3) The 1D CVCNN model performs better than the 1D CNN in the noise interference environment. The model shows more robustness to noise, this makes the 1D CVCNN model much more applicable in practical applications.

The 1D CVCNN model can diagnose OC fault accurately under noisy signals environment and no other noise reduction needed. The experimental results show that the 1D CVCNN is more superior to the existing traditional methods. At present, 1D CVCNN is first utilized to diagnose fault of inverter-fed motor drives. we think that the method does not rely on system architecture or control methods

The limitation of the proposed model is that the training time is longer than other methods, the main reason is that the operation of complex-valued convolution needs more time. In the future, we will study more on one dimensional complex-value CNN to reducing training time. The method may have some other unknown problems. In the future, we will spend more time to study these unknown problems, and develop a perfect set of solutions.

REFERENCES

[1] P. Wikstrom, L. A. Terens, and H. Kobi, "Reliability, availability, and maintainability of high-power variable-speed drive systems," *IEEE Trans. Ind. Appl.*, vol. 36, no. 1, pp. 231–241, Jan. 2000.

[2] F. W. Fuchs, "Some diagnosis methods for voltage source inverters in variable speed drives with induction machines a survey," in *Proc. IECON 29th Annu. Conf. IEEE Ind. Electron. Soc.*, vol. 2, Nov. 2003, pp. 1378–1385.

[3] B. Wang, J. Wang, B. Sen, A. Griffo, Z. Sun, and E. Chong, "A fault-tolerant machine drive based on permanent magnet-assisted synchronous reluctance machine," *IEEE Trans. Ind. Appl.*, vol. 54, no. 2, pp. 1349–1359, Mar. 2018.

[4] J. O. Estima and A. J. M. Cardoso, "A new algorithm for real-time multiple open-circuit fault diagnosis in voltage-fed PWM motor drives by the reference current errors," *IEEE Trans. Ind. Electron.*, vol. 60, no. 8, pp. 3496–3505, Aug. 2013.

[5] I. Jlassi, J. O. Estima, S. K. El Khil, N. M. Bellaaj, and A. J. M. Cardoso, "A robust observer-based method for IGBTs and current sensors fault diagnosis in voltage-source inverters of PMSM drives," *IEEE Trans. Ind. Appl.*, vol. 53, no. 3, pp. 2894–2905, May 2017.

[6] S. Shao, P. W. Wheeler, J. C. Clare, and A. J. Watson, "Fault detection for modular multilevel converters based on sliding mode observer," *IEEE Trans. Power Electron.*, vol. 28, no. 11, pp. 4867–4872, Nov. 2013.

[7] D. U. Campos-Delgado and D. R. Espinoza-Trejo, "An observer-based diagnosis scheme for single and simultaneous open-switch faults in induction motor drives," *IEEE Trans. Ind. Electron.*, vol. 58, no. 2, pp. 671–679, Feb. 2011.

[8] Q.-T. An, L. Sun, and L.-Z. Sun, "Current residual vector-based open-switch fault diagnosis of inverters in PMSM drive systems," *IEEE Trans. Power Electron.*, vol. 30, no. 5, pp. 2814–2827, May 2015.

[9] J. Poon, P. Jain, I. C. Konstantakopoulos, C. Spanos, S. K. Panda, and S. R. Sanders, "Model-based fault detection and identification for switching power converters," *IEEE Trans. Power Electron.*, vol. 32, no. 2, pp. 1419–1430, Feb. 2017.

[10] H. Zhao and L. Cheng, "Open-switch fault-diagnostic method for back-to-back converters of a doubly fed wind power generation system," *IEEE Trans. Power Electron.*, vol. 33, no. 4, pp. 3452–3461, Apr. 2018.

[11] J.-H. Choi, S. Kim, D. S. Yoo, and K.-H. Kim, "A diagnostic method of simultaneous open-switch faults in inverter-fed linear induction motor drive for reliability enhancement," *IEEE Trans. Ind. Electron.*, vol. 62, no. 7, pp. 4065–4077, Jul. 2015.

[12] C. Choi and W. Lee, "Design and evaluation of voltage measurement-based sectoral diagnosis method for inverter open switch faults of permanent magnet synchronous motor drives," *IET Electr. Power Appl.*, vol. 6, no. 8, p. 526, 2012.

[13] X. Wu, C.-Y. Chen, T.-F. Chen, S. Cheng, Z.-H. Mao, T.-J. Yu, and K. Li, "A fast and robust diagnostic method for multiple open-circuit faults of voltage-source inverters through line voltage magnitudes analysis," *IEEE Trans. Power Electron.*, vol. 35, no. 5, pp. 5205–5220, May 2020.

[14] C. Zhang, Y. He, T. Yang, B. Zhang, and J. Wu, "An analog circuit fault diagnosis approach based on improved wavelet transform and MKELM," *Circuits, Syst., Signal Process.*, vol. 41, no. 3, pp. 1255–1286, Mar. 2022.

[15] B. Cai, Y. Zhao, H. Liu, and M. Xie, "A data-driven fault diagnosis methodology in three-phase inverters for PMSM drive systems," *IEEE Trans. Power Electron.*, vol. 32, no. 7, pp. 5590–5600, Jul. 2017.

[16] T. Wang, H. Xu, J. Han, E. Elbouchikhi, and M. E. H. Benbouzid, "Cascaded H-bridge multilevel inverter system fault diagnosis using a PCA and multiclass relevance vector machine approach," *IEEE Trans. Power Electron.*, vol. 30, no. 12, pp. 7006–7018, Dec. 2015.

[17] S. S. Moosavi, A. Djerdir, Y. Ait-Amirat, D. A. Khaburi, and A. N'Diaye, "Artificial neural network-based fault diagnosis in the AC–DC converter of the power supply of series hybrid electric vehicle," *IET Electr. Syst. Transp.*, vol. 6, no. 2, pp. 96–106, Jun. 2016.

[18] T. Wang, J. Qi, H. Xu, Y. Wang, L. Liu, and D. Gao, "Fault diagnosis method based on FFT-RPCA-SVM for cascaded-multilevel inverter," *ISA Trans.*, vol. 60, pp. 156–163, Jan. 2016.

[19] Y. Xia and Y. Xu, "A transferrable data-driven method for IGBT open-circuit fault diagnosis in three-phase inverters," *IEEE Trans. Power Electron.*, vol. 36, no. 12, pp. 13478–13488, Dec. 2021.

[20] K. Barrera-Llanga, J. Burriel-Valencia, Á. Sapena-Bañó, and J. Martínez-Román, "A comparative analysis of deep learning convolutional neural network architectures for fault diagnosis of broken rotor bars in induction motors," *Sensors*, vol. 23, no. 19, p. 8196, Sep. 2023, doi: 10.3390/s23198196.

[21] C. Lu, Z. Wang, and B. Zhou, "Intelligent fault diagnosis of rolling bearing using hierarchical convolutional network based health state classification," *Adv. Eng. Informat.*, vol. 32, pp. 139–151, Apr. 2017.

[22] L. Wen, X. Li, L. Gao, and Y. Zhang, "A new convolutional neural network-based data-driven fault diagnosis method," *IEEE Trans. Ind. Electron.*, vol. 65, no. 7, pp. 5990–5998, Jul. 2018.

[23] D. T. Hoang and H. J. Kang, "A motor current signal-based bearing fault diagnosis using deep learning and information fusion," *IEEE Trans. Instrum. Meas.*, vol. 69, no. 6, pp. 3325–3333, Jun. 2020.

[24] W. Gong, H. Chen, Z. Zhang, M. Zhang, and H. Gao, "A data-driven-based fault diagnosis approach for electrical power DC–DC inverter by using modified convolutional neural network with global average pooling and 2-D feature image," *IEEE Access*, vol. 8, pp. 73677–73697, 2020.

[25] Q. Sun, X. Yu, H. Li, and J. Fan, "Adaptive feature extraction and fault diagnosis for three-phase inverter based on hybrid-CNN models under variable operating conditions," *Complex Intell. Syst.*, vol. 8, no. 1, pp. 29–42, Feb. 2022.

[26] T. Ince, S. Kiranyaz, L. Eren, M. Askar, and M. Gabbouj, "Real-time motor fault detection by 1-D convolutional neural networks," *IEEE Trans. Ind. Electron.*, vol. 63, no. 11, pp. 7067–7075, Nov. 2016.

[27] C. Wu, P. Jiang, C. Ding, F. Feng, and T. Chen, "Intelligent fault diagnosis of rotating machinery based on one-dimensional convolutional neural network," *Comput. Ind.*, vol. 108, pp. 53–61, Jun. 2019.

[28] S. Zhang, R. Wang, Y. Si, and L. Wang, "An improved convolutional neural network for three-phase inverter fault diagnosis," *IEEE Trans. Instrum. Meas.*, vol. 71, pp. 1–15, 2022.

[29] W. Yuan, Z. Li, Y. He, R. Cheng, L. Lu, and Y. Ruan, "Open-circuit fault diagnosis of NPC inverter based on improved 1-D CNN network," *IEEE Trans. Instrum. Meas.*, vol. 71, pp. 1–11, 2022.

[30] J. Zhang and Y. Wu, "Complex-valued unsupervised convolutional neural networks for sleep stage classification," *Comput. Methods Programs Biomed.*, vol. 164, pp. 181–191, Oct. 2018.

[31] S. Rawat, K. P. S. Rana, and V. Kumar, "A novel complex-valued convolutional neural network for medical image denoising," *Biomed. Signal Process. Control*, vol. 69, Aug. 2021, Art. no. 102859.

[32] R. Peuget, S. Courtine, and J.-P. Rognon, "Fault detection and isolation on a PWM inverter by knowledge-based model," *IEEE Trans. Ind. Appl.*, vol. 34, no. 6, pp. 1318–1326, Nov. 1998.

[33] S. Chen, J. Yu, and S. Wang, "One-dimensional convolutional neural network-based active feature extraction for fault detection and diagnosis of industrial processes and its understanding via visualization," *ISA Trans.*, vol. 122, pp. 424–443, Mar. 2022.

[34] S. Kiranyaz, A. Gastli, L. Ben-Brahim, N. Alemadi, and M. Gabbouj, "Real-time fault detection and identification for MMC using 1D convolutional neuralnetworks," *IEEE Trans. Ind. Electron*, vol. 66, no. 11, pp. 8760–8771, Nov. 2019.

[35] S. Kiranyaz, O. Avci, O. Abdeljaber, T. Ince, M. Gabbouj, and D. J. Inman, "1D convolutional neural networks and applications: A survey," *Mech. Syst. Signal Process.*, vol. 151, Apr. 2021, Art. no. 107398.

[36] Q. Chao, J. Tao, X. Wei, Y. Wang, L. Meng, and C. Liu, "Cavitation intensity recognition for high-speed axial piston pumps using 1-D convolutional neural networks with multi-channel inputs of vibration signals," *Alexandria Eng. J.*, vol. 59, no. 6, pp. 4463–4473, Dec. 2020.

[37] H. Wang, J. Xu, R. Yan, and R. X. Gao, "A new intelligent bearing fault diagnosis method using SDP representation and SE-CNN," *IEEE Trans. Instrum. Meas.*, vol. 69, no. 5, pp. 2377–2389, May 2020.

[38] F. Zou, H. Zhang, S. Sang, X. Li, W. He, X. Liu, and Y. Chen, "An anti-noise one-dimension convolutional neural network learning model applying on bearing fault diagnosis," *Measurement*, vol. 186, Dec. 2021, Art. no. 110236.

[39] L. Jing, M. Zhao, P. Li, and X. Xu, "A convolutional neural network based feature learning and fault diagnosis method for the condition monitoring of gearbox," *Measurement*, vol. 111, pp. 1–10, Dec. 2017.

[40] L. Yu, Y. Hu, X. Xie, Y. Lin, and W. Hong, "Complex-valued full convolutional neural network for SAR target classification," *IEEE Geosci. Remote Sens. Lett.*, vol. 17, no. 10, pp. 1752–1756, Oct. 2020.

[41] E. López-Jiménez, J. I. Vasquez-Gomez, M. A. Sanchez-Acevedo, J. C. Herrera-Lozada, and A. V. Uriarte-Arcia, "Columnar cactus recognition in aerial images using a deep learning approach," *Ecolog. Informat.*, vol. 52, pp. 131–138, Jul. 2019.

[42] K. Ghiasi-Shirazi, "Competitive cross-entropy loss: A study on training single-layer neural networks for solving nonlinearly separable classification problems," *Neural Process. Lett.*, vol. 50, no. 2, pp. 1115–1122, Oct. 2019.
[43] N. Guberman, "On complex valued convolutional neural networks," 2016, *arXiv:1602.09046*.
[44] Z. Zhang, H. Wang, F. Xu, and Y.-Q. Jin, "Complex-valued convolutional neural network and its application in polarimetric SAR image classification," *IEEE Trans. Geosci. Remote Sens.*, vol. 55, no. 12, pp. 7177–7188, Dec. 2017.
[45] X. Yao, X. Shi, and F. Zhou, "Human activities classification based on complex-value convolutional neural network," *IEEE Sensors J.*, vol. 20, no. 13, pp. 7169–7180, Jul. 2020.
[46] F. Cai, M. Zhan, Q. Chai, and J. Jiang, "Fault diagnosis of DAB converters based on ResNet with adaptive threshold denoising," *IEEE Trans. Instrum. Meas.*, vol. 71, pp. 1–10, 2022.

BOWEN CUI received the B.S. degree in mechanical engineering from the Southwestern University of Science and Technology, Mianyang, China, in 1988, and the M.S. degree in mechanical engineering and the Ph.D. degree in electrical engineering from Northwestern Polytechnical University, Xi'an, China, in 1994 and 2002, respectively. From September 2015 to September 2016, he was a Visiting Scholar with the Department of Electrical Engineering and Computer Science, The University of Tennessee at Knoxville, Knoxville, TN, USA. He is currently a Professor of electrical engineering with the School of Marine Engineering, Jimei University. His current research interests include modern signal processing and machine learning algorithms for power electronics system fault diagnosis.

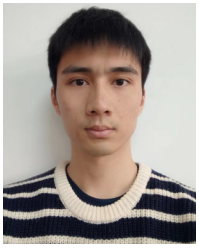

SIYUAN ZHANG was born in Anhui, China, in 1998. He received the B.S. degree in mechanical engineering from Anhui University of Architecture, Hefei, China, in 2021. He is currently pursuing the M.S. degree in marine and ocean engineering with Jimei University, Xiamen, China. His research interest includes machine learning and its application to fault diagnosis of power electronics converter.

JIAYI SU was born in Sichuan, China, in 1995. She received the B.S. degree in electrical engineering from Xihua University, Chengdu, China, in 2019, and the M.S. degree in electrical engineering from Jimei University, Xiamen, China, in 2022. She is currently working in the field of photovoltaic new energy inverters. Her research interests include fault diagnosis of marine inverters and deep learning neural network algorithms.

HUAMIN CUI was born in Anhui, China, in 1995. He received the B.S. degree in electrical engineering from Qingdao University of Technology, Qingdao, China, in 2019, and the M.S. degree in electrical engineering from Jimei University, Xiamen, China, in 2023. His research interest includes machine learning and its application to fault diagnosis of power electronics converter.